Nuclear Inst. and Methods in Physics Research, A 977 (2020) 164295

Contents lists available at ScienceDirect

Nuclear Inst. and Methods in Physics Research, A

journal homepage: www.elsevier.com/locate/nima

In-depth evaluation of TOF-PET detectors based on crystal arrays and the TOFPET2 ASIC

Efthymios Lamprou *, Filomeno Sanchez, Jose M. Benlloch, Antonio J. Gonzalez

Instituto de Instrumentación para Imagen Molecular (I3M), Centro Mixto CSIC—Universitat Politècnica de València, 46022 Valencia, Spain

ARTICLE INFO

Keywords:
TOF-PET
ASIC
Time walk
Crystal arrays
SiPM
Timing resolution

ABSTRACT

In recent years high efforts have been devoted to enhance spatial and temporal resolutions of PET detectors. However, accurately combining these two main features is, in most of the cases, challenging. Typically, a compromise has to be made between the number of readout channels, scintillator type and size, and photosensors arrangement if aiming for a good system performance, while keeping a moderate cost. In this work, we have studied several detector configurations for PET based on a set of 8×8 Silicon Photomultiplier (SiPMs) of 3×3 mm^2 active area, and LYSO crystal arrays with different pixel sizes. An exhaustive evaluation in terms of spatial, energy and timing resolution was made for all detector configurations. In some cases, when using pixel sizes different than SiPM active area, a significant amount of scintillation light may spread among several SiPMs. Therefore, we made use of a calibration method considering the different SiPM timing contributions. Best Detector Time Resolution (DTR) of 156 ps FWHM was measured when using 3×3 mm^2 crystal pixels directly coupled to the 3×3 mm^2 SiPMs. However, when using 1.5 mm crystal pixels with the same photosensor array, although we could clearly resolve all crystal pixels, an average DTR of 250 ps FWHM was achieved. We also shed light in this work on the timing dependency of the crystal pixel and photosensor alignment.

1. Introduction

During the last years, the overall performance of Positron Emission Tomography (PET), including Time-OF-Flight (TOF) technique, has significantly improved, facilitating the diagnostic and therapy assessment processes in several medical fields (e.g. oncology, cardiology, neurology etc.) [1]. The main requirements for a PET system, from the clinical point of view, have been high sensitivity allowing one to significantly reduce the administered dose and/or the scanning time, and good spatial resolution. However, more recently, accurate timing resolution is also feasible, resulting in a highly increased Signal-to-Noise Ratio (SNR) of reconstructed images [2,3]. Those parameters are directly related to the detector configuration. The introduction of Silicon Photomultiplier (SiPMs) along with the rapid progress of electronics and the improvements in scintillation materials have allowed the development of high-resolution PET detectors with accurate timing capabilities [3–5].

Several detector configurations have been suggested over the years achieving an excellent spatial resolution. In terms of scintillator geometry, monolithic blocks or crystal arrays have been proposed [6,7]. Indeed, the particular configuration of choice and the crystal type (LYSO, BGO, GAGG, etc.) impacts the timing capabilities of the detector block [3]. This dependency is mainly related to the emission and collection of scintillation light [8,9]. In order to reach accurate time resolution in PET detectors, a sharp rise time of the scintillation pulse and, thus, a high number of photons in a very short time is mandatory [3,8]. Configurations in which the collection of the scintillation light produced by a single gamma ray is carried out by multiple photosensors (light sharing approaches) typically show a more challenging determination of the impact time tag [8]. On the contrary, in detector configurations where the crystal pixel size is smaller (and centered) or matched to the photosensor element size, typically the best results in time resolution are found. This occurs since most pf generated scintillation photons are collected by only one photosensor element with no significant light losses. Unfortunately, if aiming to combine very high spatial and timing resolution using this one-to-one detector approach, a large amount of photosensors and readout channels would be required, meaning a high detector cost.

In this work, crystal arrays of various pixel sizes are evaluated when coupled to the same array of SiPM. This work aims to shed light on different detector configurations, suitable for TOF-PET systems. The current analysis provides a better understanding of the light sharing effect when using crystal arrays, the limitations that show up but also possible ways to compensate them.

* Corresponding author.
E-mail address: e.lamprou@i3m.upv.es (E. Lamprou).

https://doi.org/10.1016/j.nima.2020.164295
Received 3 March 2020; Received in revised form 15 June 2020; Accepted 21 June 2020
Available online 24 June 2020

2. Materials and methods

2.1. Scintillators

Three types of LYSO crystal arrays (EPIC Crystal, Kunshan, China) were used during the experiments, all with 10 mm thickness but different pixel sizes (Fig. 1). One was composed by 8×8 crystal pixels of 3×3 mm^2 and 3.36 mm pitch using $BaSO_4$ as a separator between pixels while Enhanced Specular Reflectors (ESR) of 65 μm, was used on all lateral faces and the entrance (Fig. 1 left). The second block had 12×12 pixels of 2×2 mm^2 size and 2.08 mm pitch (Fig. 1 center) and the third array had 17×17 pixels of 1.5×1.5 mm^2 and 1.58 mm pitch (Fig. 1 right). Additionally, for 2 and 1.5 mm pixel sizes, entrance and lateral faces for all crystal pixels were covered with ESR of 65 μm.

2.2. ASIC readout & SiPM photosensors

The crystal arrays were optically coupled using optical grease to SiPM arrays. In particular, we used two arrays of 8×8 elements, 3×3 mm^2 active area, and 3.36 mm pitch of the type PA3325 from KETEK (Munich, Germany). These arrays, were biased at 28.7 V (4 V over the breakdown voltage). The frontend electronics selected to read out all SiPM signals were based on the commercially available Application Specific Integrated Circuit (ASIC) named TOFPET2 from PETsys (Lisbon, Portugal) [10]. Each ASIC reads out 64 signals and integrates high resolution Time-To-Digital converters (30 ps binning) as well as charge integrators for each channel, permitting in that way a quite accurate decoding of gamma-ray pulses.

2.3. Detector configurations and set-up

First, two identical detectors based on crystal arrays of 3×3 mm^2 size were tested. Thus, each crystal pixel perfectly matched with the photosensor element, resulting in the so-called one-to-one coupling. These detectors were tested in coincidence mode, initially for calibration (see below Section 2.4) and then for evaluation purposes. Afterwards, one of these detectors was exchanged for the other configuration types, as it will be described below.

When using crystal arrays with 2×2 mm^2 and 1.5×1.5 mm^2 pixel sizes, that means smaller crystal pitch than the photosensor active area, this resulted in the previously described light sharing configuration. Optical light guides in between the crystal and the sensor were not utilized, except for an additional measurement with the 1.5 mm pixels. In particular, a 1 mm thick polished glass layer was added. A more detailed description of the light distribution for all three detector configurations is provided in the results section.

All coincidence measurements were carried having the detectors at a distance of 15 cm, and were long enough, in order to avoid statistical fluctuations, that might affect the accuracy of the extrapolated data. A stable temperature environment was ensured in all experiments at 18 °C (±1 °C). We used a small size ^{22}Na source with 1 mm in diameter and an activity of 470 kBq, centered in a plastic disk of 1 inch in diameter and 6 mm height.

2.4. System calibration

Since the main aim of the experiments was the evaluation of the timing capabilities of each configuration, the correction of the timing skew is critical, which refers to the variations in the time-paths among channels [8]. In order to correct this effect, the two detectors based on the crystal arrays with 3×3 mm^2 pixel size were used in coincidence. Two measurements were carried out, first with the source attached to one detector and then to the other one. In both measurements the source was centered into one pixel, using a mechanical holder. Therefore, each detector was completely irradiated in coincidence mode with only one channel in the opposite detector (reference detector). We determined the Gaussian centroids of the time differences among all channel pairs of the two detectors (a total of 64 per detector). These values were stored in look-up-tables. This information is unique for each channel and was used as an offset calibration in all following timestamps recordings, independently of the coupled scintillation block, since photosensor array and corresponding ASIC remain the same.

After the skew correction, a time walk calibration was also investigated [8]. The aim was to improve the uncertainties in the timestamp generation related to the signal level. This correction is of special importance when a significant amount of scintillation light is spread among multiple channels, such as in the case of the 2 and 1.5 mm pixel sizes, due to their geometrical mismatches with the photosensor array. The acquired data were first energy filtered using a 450–572 keV photopeak energy window. Then, we generated 2D plots for each channel of the time difference of its earliest recorded timestamp with the one recorded by the reference detector, as a function of its collected energy. In these 2D plots, projections to the time difference axis were made in very small energy bands. The profiles were fitted with Gaussian distributions, returning for each selected energy band its centroid (and standard deviation), corresponding to a time offset related to the time walk uncertainty. Thus, a time walk calibration file was obtained for each of the detector configurations.

2.5. Thresholds scan

Different thresholds can be configured in the TOFPET2 ASIC which impact the timing performance. We carried out an optimization of the so-called *vth_t1* threshold, which is directly related to the timestamp generation of each pulse. This task was carried out for all configurations, after applying the time skew correction in the recorded data.

2.6. Timing, position and energy estimation. Timestamp averaging method

As it was mentioned above, in addition to the Coincidence Time Resolution (CTR), an evaluation of the spatial and energy resolution of each detector was performed. All results, timing and position related, were obtained after applying a 450–572 keV photopeak energy window. Energy resolution was calculated, after linearity correction, as the ratio of the FWHM to the distribution centroid. Regarding the position estimation, it was obtained by applying the Center-Of-Gravity (COG) algorithm:

$$x = \frac{\sum_{i=0}^{i=n} xi \cdot Ei}{Ei}, \quad y = \frac{\sum_{i=0}^{i=n} yi \cdot Ei}{Ei},$$

where xi and yi are the photosensor positions and Ei the collected charge. The total energy was obtained as the sum of channels with an Ei value over the threshold. Regarding the determination of the timing information, when multiple channels (timestamps) are involved, it has been suggested to use the average of timestamps and in particular of weighted averaging methods, instead of assigning the timing to the earliest recorded one [8,11]. Herein, for the configuration using the 2 and 1.5 mm pixels arrays (Sections 3.4–3.6), an energy weighted averaging method using the first n channel timestamps (T_i) was also used to assign the timestamp to each event:

$$t_{ev} = \frac{\sum_{i=0}^{i=n} Ti \cdot Ei}{Ei}$$

3. Results

3.1. Time skew correction

Fig. 2 shows the time differences among all 64 channels of 1 ASIC, related to the reference one, before and after calibration of the skew time error, respectively. As it can be observed, significant variations in the Gaussian centroids were found, with the deviations inside one single ASIC as large as 1.6 ns.

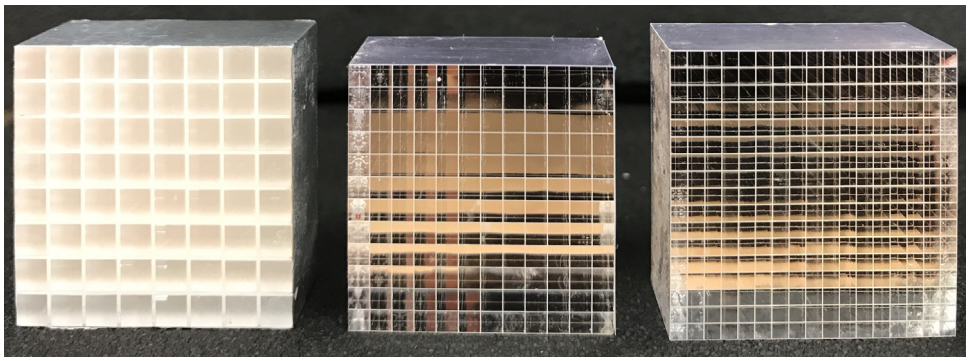

Fig. 1. Left, crystal array with pixel size 3×3 mm^2. Center, crystal array with pixel size 2×2 mm^2. Right, crystal array with pixel size of 1.5×1.5 mm^2.

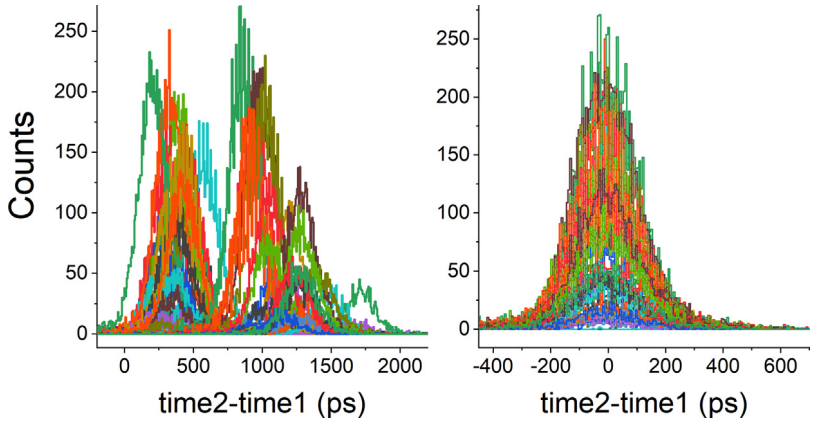

Fig. 2. Left, measured Gaussian centroids of the timing distributions among all 64 ASIC channel pairs (represented by different colors), related to one single channel of the opposite detector (reference detector). Right, time skew correction shifting all Gaussian centroids to 0. (For interpretation of the references to color in this figure legend, the reader is referred to the web version of this article.)

3.2. Threshold scan

After the time skew correction, we obtained the average (whole detector) CTR values as a function of the threshold value for the four tested configurations namely crystal pixels of 3 mm section, 2 mm, 1.5 mm and 1.5 mm with the optical window. Fig. 3 depicts the results for the four cases. For the case using 3 mm pixel size, we did not observe any significant threshold dependency across *vth_t1* values. Best results were obtained when using the value of 15 DAQ units, providing an average CTR of 238 ± 6 ps FWHM (standard deviation of 11 ps) for impacts across the whole detector.

In the case of the 2 mm pixels, the best average time resolution for all channels was measured using the time threshold corresponding to 7 DAQ units and was found to be 460 ± 7 ps FWHM (standard deviation of 21 ps), before time walk correction. It is observed that 7 ADC units provides the best CTR, but similar values are obtained for the range of 6 to 9 DAQ units.

Similarly to the case of 2 mm pixels, when testing the 1.5 mm pixels, best CTR values were found for 6–7 DAQ units (Fig. 3 bottom-left). Considering that the difference in terms of timing resolution between 6 and 7 DAQ units, is inside the estimated error and aiming to avoid even lower threshold that might result to more signal jitter or false triggering, the threshold of 7 DAQ units was selected to be used in all following measurements. For this threshold configuration, the average time resolution before time walk correction, was measured to be 455 ± 11 ps FWHM (standard deviation of 22 ps). When measuring with the 1.5 mm pixels adding the optical light guide, the average CTR exhibited a similar tendency. The best CTR value was now found to be 460 ± 10 ps FWHM (standard deviation of 28 ps) at a threshold of 8 DAQ units. For this configuration, again we observed a worsening of the CTR for very low thresholds.

3.3. Analysis for crystals with 3×3 mm^2 pixels

In the detectors based on the one-to-one coupling approach, we observed that on average, 80% of the generated optical photons for each gamma-ray impact are collected by a single photosensor element, resulting in a sharp rise time of the signal. This suggests to only use the information of one channel for the timing and energy determination.

As depicted in Fig. 4 left, 2D flood maps of the crystal array were generated aiming to study the spatial resolution as well as the CTR for several Regions of Interests (ROIs). Regarding the spatial resolution, all pixels are well resolved, providing a detector spatial resolution of 3 mm. We also analyzed the peak-to-valley ratio obtaining 936 ± 68 and on average one count per bin between peaks.

ROIs for each crystal pixel in one column were made to study the energy and timing resolution as a function of the pixel position. Regarding the energy resolution, we found an average energy resolution for all pixels in that column of 11.4% with a standard deviation of 0.7%, after correction for the SiPM saturation. Fig. 4 right shows the energy spectra of one pixel belonging to this column.

Fig. 5 shows the measured CTR as a function of the pixel position in the same selected column after applying the energy window filter. The sketch on the top depicts the relative crystal pixel and SiPM positions. We found a homogeneous CTR across all pixels, with an average of 242 ps (standard deviation of 6 ps), and best value the 232 ± 4 ps FWHM. From the average value of 242 ps FWHM we have determined a Detector Time Resolution (DTR) of 171 ps FWHM for this detector configuration.

3.4. Analysis for crystals with 2×2 mm^2 pixels

When using the crystal arrays of 2 mm pixels coupled to 3 mm SiPM (in coincidence with the reference detector of 3 mm pixels) due to

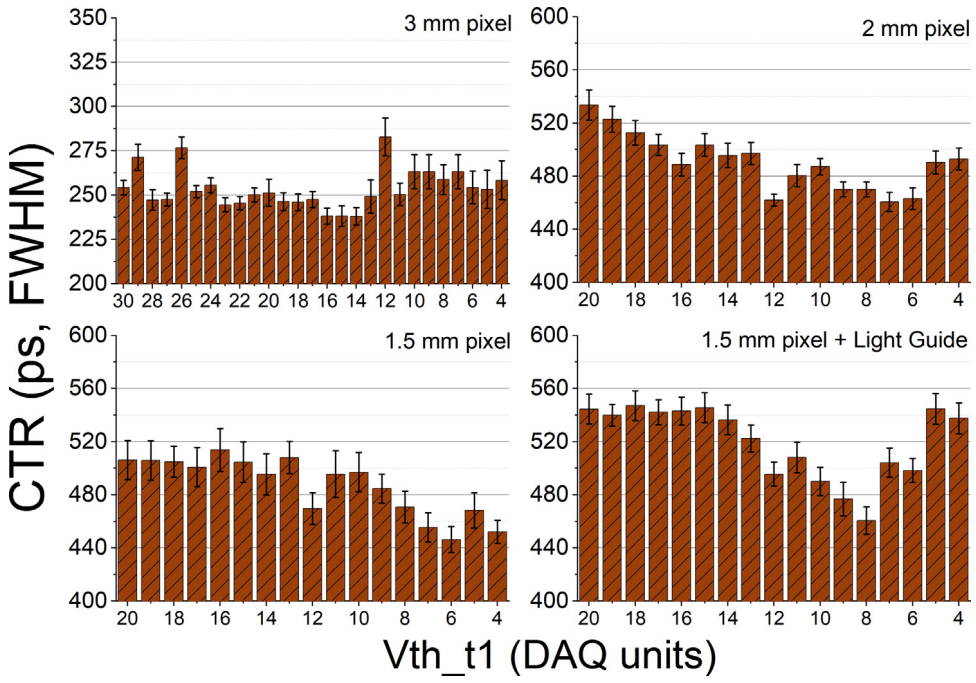

Fig. 3. Average CTR measurements for the whole detector of the four tested configurations, as a function of the threshold level *vth_t1*.

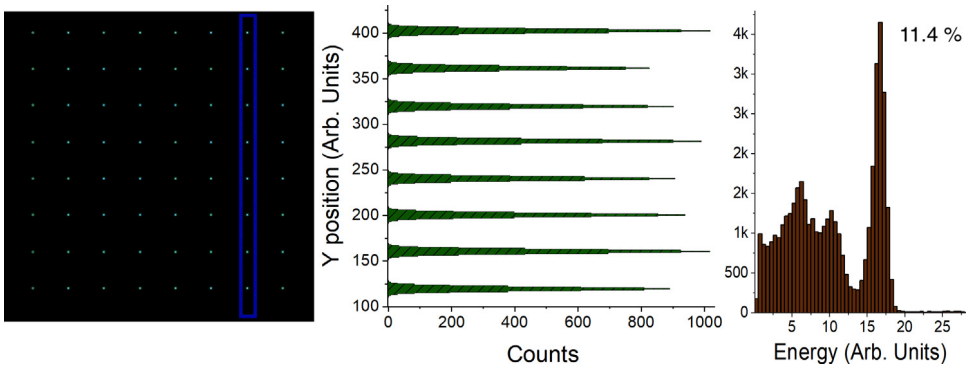

Fig. 4. Left, flood map obtained with the crystal array composed by the 3 mm crystal pixel. Center, projection data of one column of the crystal array. Right, energy spectra for a central pixel.

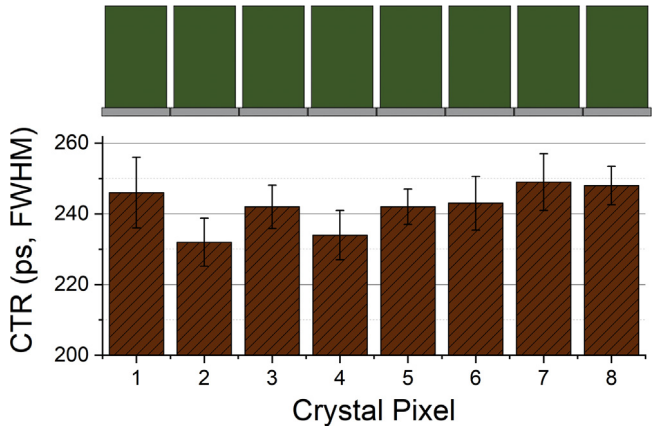

Fig. 5. Top, relative position of each crystal pixel belonging to one column, with respect to the photosensor elements. Bottom, CTR measured when filtering each crystal pixel individually.

the geometrical mismatch between them, light sharing was expected leading to the triggering of several SiPM (ASIC channels) for each gamma-ray event. During the data analysis, we measured an average of 40% of the scintillation light captured by only one SiPM while the rest was shared to surrounding photosensors. This generates a variability of signal amplitudes in multiple readout channels for each event. Moreover, lower signals are typically affected by noise during the generation of the timestamp due to the time walk error. Fig. 6 depicts the time differences of the earliest recorded timestamp with the one recorded by the reference detector, as a function of the collected charge in DAQ units for a given pair channel. As it was also described above, a calibration method was carried out to compensate the delay in the timestamp generation as a function of the signal amplitude. In a following measurement using this configuration, after correction of the timestamps for the time walk, an average timing resolution of 381 ± 6 ps FWHM was reached (for the whole detector).

Fig. 7 left exhibits all 12×12 crystal elements clearly resolved with a peak-to-valley ratio 46 ± 7. The average energy resolution for the 12 crystal elements belonging to the filtered column of crystals was found to be 11.8% with a standard deviation of 0.5%. In this case the time analysis, besides including the CTR obtained when using the earliest timestamp, we also include the results obtained when using a weighted

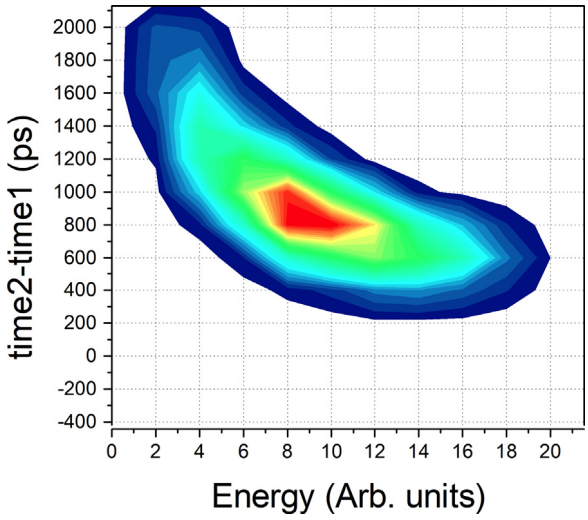

Fig. 6. Contour plot of the time differences of one pair of channels as a function of the energy of the earliest hit showing the time walk influence.

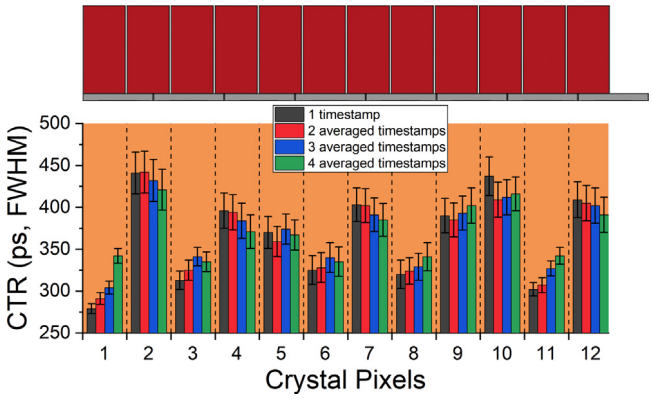

Fig. 8. Top, relative position of each crystal pixel belonging to one column, with respect to the photosensor elements. Bottom, CTR for each crystal pixel, obtained using the earliest timestamp and an average energy weighting timestamp method after applying a position (ROI) and energy filter.

by energy averaging method. As it can be appreciated in Fig. 8, when using one timestamp, the measured CTR for this group of pixels, varies from 279 ± 6 ps to 441 ± 25 ps FWHM with an average value of 365 ps FWHM (standard deviation of 55 ps). These variations among pixels, are related to each pixel position and, thus, the light collection efficiency. The weighted averaging method, although did not provide better average values compared to the use of 1 timestamp, it reduces the standard deviation among pixels, being 32 ps for the case of 4 weighted timestamps (average value 370 ps FWHM).

3.5. Analysis for crystals with 1.5×1.5 mm^2 pixels

The crystal array with 1.5 mm pixels was coupled to the photosensor array without any optical guide in between, despite the small crystal pixel size compared to the photosensor pitch (3.36 mm). As depicted in Fig. 9 left, all 17×17 crystal elements were resolved. After again applying the ROI filtering for a column of pixels, a peak-to-valley of 7 ± 1 was measured. However, some deterioration is observed at the detector block edges due to a poorer light collection. The average energy resolution for the filtered column was found to be 13% with a standard deviation of 1% (see Fig. 9 right).

The time walk correction was also applied to these data, following the methodology described above. In a measurement using this configuration, the average time resolution for the whole detector block after the time walk correction was found to be 365 ± 4 ps FWHM. A more detailed time analysis for the 17 crystal pixels contained in one column of the crystal array was carried out, again using the earliest timestamp as well as the energy weighted averaging method. As it can be seen in Fig. 10, when using one timestamp values as good as 241 ± 5 ps FWHM were achieved for crystals whose exit face was fully contained to just one photosensor element. In contrast to this, pixels which were coupled in between several photosensor elements, showed worse time resolution reaching 370 ± 23 ps FWHM. Eventually, an average CTR of 303 ps FWHM (standard deviation of 37 ps) could be obtained for this detector configuration and this column of pixels. In the case of the weighted averaging method, best results were found when 3 timestamps are averaged. Although the average CTR among pixel remained 303 ps FWHM (as in the case of the earliest timestamp) the standard deviation in this case slightly improved to 26 ps.

3.6. Analysis for crystals with 1.5×1.5 mm^2 pixels and optical light guide

The crystal array with 1.5 mm pixels was also tested using a glass layer of 1 mm thick in between the scintillator and photosensor array (coupled using optical grease). The aim was to improve the spatial resolution near the detector block edges. The use of an optical guide allows one for a better pixel identification, as it generates a wider scintillation light spread. As it can be seen in Fig. 11 left, all pixels are again resolved, including the crystal edges. Moreover, there is a better homogeneity in the pixel identification, in contrast to the case without the glass window where pixels tend to concentrate within the SiPM center. Using this configuration, we determined an average peak-to-valley ratio of 9.5 ± 1.6. An average energy resolution measured for each of the studied 17 crystal elements contained in one column, was found to be 12.5% with a standard deviation of 0.7%.

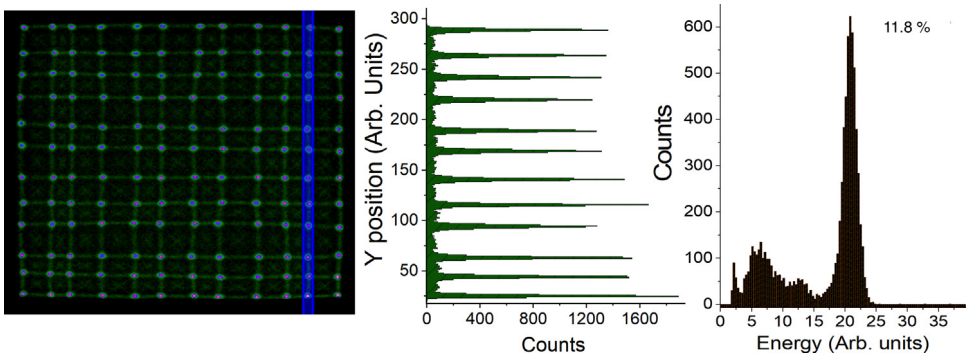

Fig. 7. Left, flood map obtained with the crystal array of 2 mm pixels. Center, projection of one column of the crystal array. Right, energy profile for the one pixel belonging to the filtered ROI.

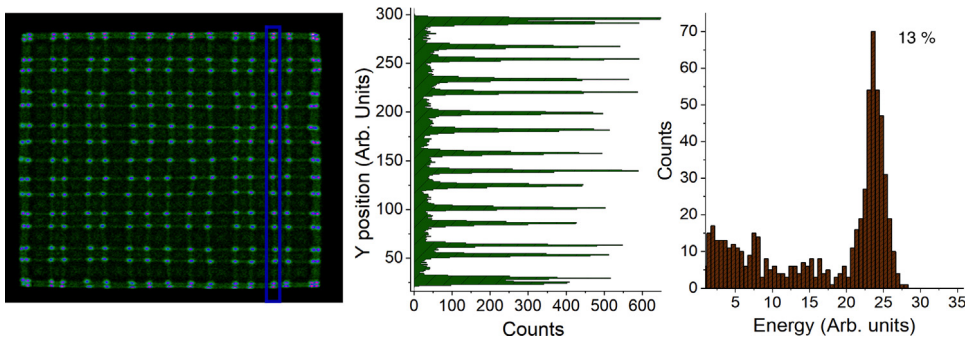

Fig. 9. Left, flood map obtained with the crystal array composed by the 1.5 mm crystal pixel. Center, projection of one column of the crystal array. Right, energy profile for one pixel belonging to the filtered column.

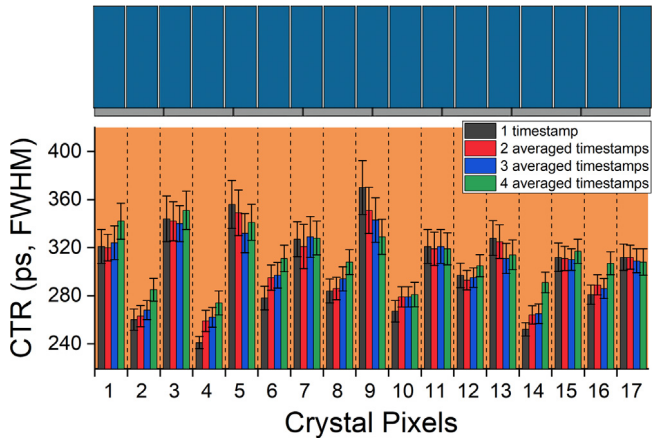

Fig. 10. Top, relative position of each crystal pixel belonging to one column, with respect to the photosensor elements. Bottom, CTR for each crystal pixel measured with the first timestamp recorded as well as with weighted averaging method, after applying an energy and position (ROI) filter.

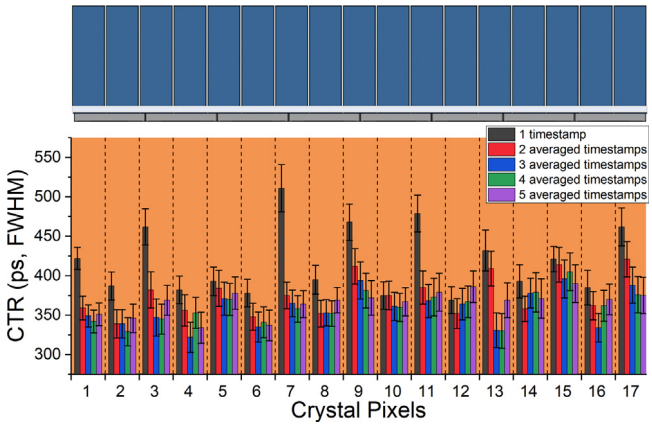

Fig. 12. Top, relative position of each crystal pixel belonging to one column, with respect to the SiPMs. Bottom, time resolution measured for each crystal pixel (after applying the energy and ROI filter), using the first corrected timestamp and an energy weighted averaging method.

Regarding the timing resolution, the use of the optical window might affect the single channel SNR and, consequently the CTR. In a following measurement, after correcting for the time walk, the average detector timing resolution was found to be 428 ± 7 ps FWHM. Then, the CTR was determined after applying the positioning (ROI) filter for all 17 pixels contained in one column. The first timestamp recorded and a weighted by energy averaging method was again used, expecting some improvement compared to the only one timestamp due to the more intense light sharing. As the analysis revealed, when using four timestamps, better timing performance was found. In particular for the cases of 1, 2, 3, 4 and 5 timestamps, time resolutions of 418 ± 43, 376 ± 26, 358 ± 23, 360 ± 20 and 367 ± 16 ps were obtained, respectively. That being said, averaging weighted timestamps, contributed to the improvement of both of the average value of pixels as well as in the deviation among them. Fig. 12 shows the CTR as a function of the pixel position and for different number of averaged weighted timestamps.

4. Discussion

In terms of spatial resolution, all tested crystal pixel sizes (3 mm, 2 mm, and 1.5 mm) were resolved when coupled to 3 × 3 mm^2 photosensor arrays. Additionally, we observed that small crystals of 1.5 mm were distinguishable including those at the edges, although

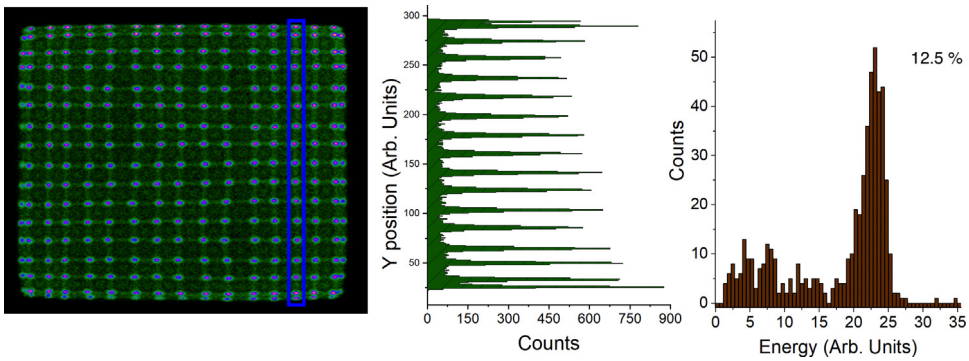

Fig. 11. Left, flood map obtained with the crystal array composed by the 1.5 mm crystal pixel and optical light guide. Center, projection of one column of the crystal array. Right, energy profile for a pixel of the filtered column (energy filtered).

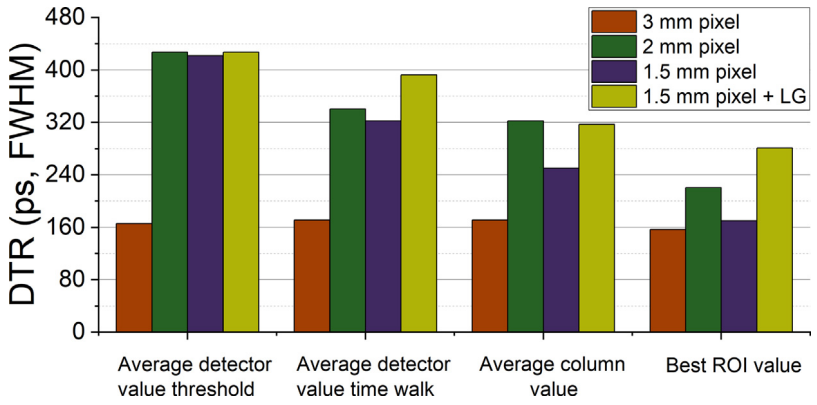

Fig. 13. Summary of measured DTR for the four tested configurations, following the optimization in terms of threshold, time walk correction and after applying positioning filters.

the last ones and in particular the pixels in the corners showed a worst peak-to-valley ratio due to the lower amount of photosensors involved in the scintillation light collection process. Significant improvement however, was observed in these regions when using the glass window. Generally, high values of the peak-to-valley ratios were found for the case of using 3 mm and 2 mm pixel, whereas lower ones were found for the rest of configurations. It is worth mentioning that in the flood map obtained with the 3 mm crystal size, hardly a background can be seen. This behavior, is expected to be a result of a combination of two factors. Firstly, the lower probability for inter-crystal-scattering compared to the cases of smaller crystal elements (1.5 and 2 mm), and secondly, the fact that a relatively high threshold was used in this configuration, resulting more improbable that the surrounding sensors collect enough photons for triggering the electronics and have an effect in the COG algorithm. Energy resolution was also evaluated during the data analysis for a group of pixels belonging in one column and, for all configurations. In general, the energy resolution of individual pixels was measured to be in the range of 11%–13% (after energy calibration).

Both average detector as well as individual crystal pixels CTR were determined for all cases. We determined first the optimum ASIC *vth_t1* threshold value for each case. When using 3 mm pixels the, dependency of the time resolution as a function of the threshold, was not found to be significant. However, best values were determined for the range between 14–16 DAQ units. All other cases seem to exhibit best values around 6–8 DAQ units. For the case of using the glass window, worst values were found for lowest DAQ values, most likely due to a poorer SNR of individual channels.

The best CTR of 232 ps was obtained with the configuration based on the one-to-one coupling approach (3 mm pixels). In the case of smaller crystal elements, scintillation light eventually spreads among few SiPMs. Indeed, we observed the CTR dependency as a function of the crystal pixel position and SiPM element. The use of an energy weighted averaging method for the timestamp determination, although it did deteriorate the average timing resolution in most of the cases, it did permit the reduction of the standard deviation among individual pixel capabilities. This approach, can be of high importance during a reconstruction process. However, as was shown above, in the case of 1.5 mm pixel and the lightguide, significant improvement was observed when 3 or 4 timestamps were used.

5. Conclusions

We have carried out a complete performance evaluation of four gamma-ray detector configurations, especially suitable for PET. Spatial, energy and timing resolution were studied in detail. The detector designs could be employed for clinical (3 mm pixels) but also for pre-clinical (1.5 mm) applications, with accurate timing capabilities.

Results showed the one-to-one coupling approach providing the best results in terms of timing and energy resolution due to, on average, a higher collection of optical photons by a single channel. Using this set-up, we have been able to reach a CTR as good as 232 ps FWHM. We are aware that alternative photosensors with improved timing capabilities using wider microcell sizes could improve these results by about 15% [12,13]. Also, the use of Ca-doped LYSO crystals could also improve the CTR by 10–20 ps FWHM [14].

When crystal pixels smaller than SiPMs active area are tested, in addition to the skew time correction, a time walk correction and, eventually, in one case the weighted averaging of several timestamps was required to provide a more accurate CTR. For the case of 2 mm crystal pixels, a CTR of 365 ps FWHM was measured for a column containing 12 crystal elements. When applying ROI filters in the crystal pixels contained in this column, we measured values equal to 279 ps. The crystal array based on the 1.5 mm pixel size, was tested with and without the use of an optical glass window of 1.0 mm thickness. As expected, the pixel identification was more homogeneous when using a glass window, including the edges, but at the cost of some CTR deterioration. In particular, for one group of pixels, an average value of 303 ps FWHM, including time walk correction, degraded to 418 ps when the light guide was used. However, this last value improves to 358 ps FWHM when the energy averaged timestamp method was used. When analyzing the CTR for a given pixel, a 241 ps FWHM was achieved without the light guide, worsening to 322 ps with the glass layer including the averaging of 3 weighted timestamps.

Since the same reference detector was used in all experiments, and its contribution was determined by the experiments described in Section 3.3, the DTR could be estimated for each case studied. In particular, the DTR for the configuration with one-to-one coupling was 171 ps FWHM. We have obtained the DTR for all configurations and processes described in this work, as shown in Fig. 13.

Summarizing, it is possible to reach good detector performance in terms of pixel identification and energy resolution, when using 3 mm photosensor arrays. The results exhibited in this work regarding spatial resolution, suggest that crystal pixels smaller than 1.5 mm could also be resolved. The time resolution however, strongly depends on the geometrical position of each crystal pixel with respect to each photosensor element. Nevertheless, even in the detector configurations in which a significant mismatch between crystal and SiPMs existed, values of CTR as low as 241 ps FWHM were achieved. Some of the proposed designs might be well suitable for the development of clinical and pre-clinical TOF-PET detectors and provide solutions for detector concepts which combine good spatial and timing resolutions.

CRediT authorship contribution statement

Efthymios Lamprou: Conceptualization, Methodology, Software, Writing - original draft. **Filomeno Sanchez:** Investigation, Validation, Supervision. **Jose M. Benlloch:** Funding acquisition, Validation, Project administration. **Antonio J. Gonzalez:** Supervision, Visualization, Validation, Writing - review & editing.

Declaration of competing interest

The authors declare that they have no known competing financial interests or personal relationships that could have appeared to influence the work reported in this paper.

Acknowledgments

This project has received funding from the European Research Council (ERC) under the European Union's Horizon 2020 research and innovation program (grant agreement No. 695536) and by the Spanish Ministerio de Economía, Industria y Competitividad under Grant TEC2016-79884-C2-1-R. The first author has also been supported by Generalitat Valenciana, Spain under grant agreement GRISOLIAP-2018-026.

References

[1] T. Jones, Townsend history and future technical innovation in positron emission tomography, J. Med. Imag. 4 (1) (2017) 011013.
[2] S. Surti, Update on time-of-flight PET imaging, J. Nucl. Med. 56 (1) (2015) 98–105.
[3] P. Lecoq, Pushing the limits in time-of-flight PET imaging, IEEE Trans. Radiat. Plasma Med. Sci. 1 (6) (2017) 473–485.
[4] S. Surti, J.S. Karp, Advances in time-of-flight PET, Phys. Med. 32 (1) (2016) 12–22.
[5] S. Gundacker, E. Auffray, K. Pauwels, P. Lecoq, Measurement of intrinsic rise times for various L(Y)SO and LuAG scintillators with a general study of prompt 728 photons to achieve 10 ps, Phys. Med. Biol. 61 (7) (2016) 2802–2837.
[6] A. González-Montoro, F. Sánchez, P. Bruyndonckx, G. Cañizares, J.M. Benlloch, A.J. González, Novel method to measure the intrinsic spatial resolution in PET detectors based on monolithic crystals, Nucl. Instrum. Methods 920 (2019) 58–67.
[7] W.W. Moses, Fundamental limits of spatial resolution in PET, Nucl. Instrum. Methods Phys. Res. A 648 (Suppl. 1) (2011) S236–S240.
[8] E. Lamprou, et al., Exploring TOF capabilities of PET detector blocks based on large monolithic crystals and analog SiPMs, Phys. Med. 70 (2020) 10–18.
[9] E. Lamprou, et al., PET Detector block with accurate 4D capabilities, Nucl. Instrum. Methods 912 (2018) 132–136.
[10] A. Di Francesco, R. Bugalho, L. Oliveira, L. Pacher, A. Rivetti, M. Rolo, et al., TOFPET2: A high-performance ASIC for time and amplitude measurements of SiPM signals in time-of-flight applications, J. Instrum. 11 (03) C03042.
[11] H.T. van Dam, G. Borghi, S. Seifert, D. Schaart, Sub-200 ps CRT in monolithic scintillator PET detectors using digital SiPM arrays and maximum likelihood interaction time estimation, Phys. Med. Biol. 58 (10) (2013) 3243–3257.
[12] V. Nadig, D. Schug, B. Weissler, V. Schulz, Evaluation Of The PETsys TOFPET2 ASIC In Multi-Channel Coincidence Experiments, arXiv:1911.08156.
[13] S. Gundacker, R.M. Turtos, E. Auffray, M. Paganoni, P. Lecoq, High-frequency SiPM readout advances measured coincidence time resolution limits in TOF-PET, Phys. Med. Biol. 64 (5) (2019).
[14] S. Gundacker, et al., State of the art timing in TOF-PET detectors with LuAG, GAGG and L(Y)SO scintillators of various sizes coupled to FBK-SiPMs, J. Instrum. 11 (2016) P08008.